Journal of Alloys and Compounds 509 (2011) 9207–9213

Contents lists available at ScienceDirect

Journal of Alloys and Compounds

journal homepage: www.elsevier.com/locate/jallcom

Fabrication and electrochemical behavior of flower-like ZnO–CoO–C nanowall arrays as anodes for lithium-ion batteries

Zhao Wu, Liming Qin, Qinmin Pan*

School of Chemical Engineering and Technology, Harbin Institute of Technology, Harbin 150001, PR China

ARTICLE INFO

Article history:
Received 10 May 2011
Received in revised form 27 June 2011
Accepted 29 June 2011
Available online 18 July 2011

Keywords:
Flower-like ZnO–CoO–C nanowall arrays
Lithium ion batteries
Electrochemical performance
Mechanism

ABSTRACT

This study reported the electrochemical performance of flower-like ZnO–CoO–C nanowall arrays as anodes of lithium-ion batteries. The arrays were fabricated through solution-immersion steps and subsequent calcination at 400 °C. At a rate of 0.5 C, the arrays exhibited a delithiation capacity of 438 mA h g^{-1} at the 50th cycle. The arrays still delivered a reversible capacity of 224 mA h g^{-1} at 2.0 C rate, much higher than those of the flower-like ZnO and ZnO–C nanowall arrays. The mechanism for the high capacity of flower-like ZnO–CoO–C nanowall arrays mainly resulted from the catalytic effect of Co phase on the decomposition of Li_2O and the conducting carbon layer formed on ZnO nanowalls. The present finding also provides a kind of nanostructured films that might be applied in solar cells and sensors, etc.

1. Introduction

Increasing demand for high-performance lithium-ion batteries (LIB) had driven people to explore novel electrode materials with high capacity and long life [1,2]. Although ZnO has a theoretical capacity of 987 mA h g^{-1} as a kind of anode material for LIB [3], its practical application is hindered by low electronic conductivity and large volume-variation of ZnO in the process of lithiation and delithiation [4–7]. In the past years, fabricating nanoscale ZnO with different dimensions and morphologies was a widely employed strategy to reduce the volume change of ZnO [8]. Among them, nanostructured ZnO films grown directly on metal substrates showed more desirable electrochemical properties compared to those of powder-form counterparts [9–13], indicating the significance of architecture (or morphology) for ZnO-based anodes.

On the other hand, deposition of carbon [14,15], metal phases (such as Ni [16], Mg [17], etc.), TiO_2 [18], or incorporation of $Ni_3ZnC_{0.7}$ [19] greatly increased the reversible capacity and cycleability of ZnO anodes due to the formation of conducting and buffering matrix between ZnO particles. Besides the conducting effect like carbon, Ni and $Ni_3ZnC_{0.7}$ phases also play a catalytic role in the conversion reaction between Li and ZnO [16,19]. More interestingly, a combination of self-supported nanostructure, catalytic and conductive effects of metal phases further improved the electrochemical performance of ZnO film-electrode. For example, flower-like ZnO–NiO–C films showed one of the highest reversible capacity and best rate capability among the reported ZnO-based anodes [20].

To further investigate the catalytic effect of metal phase on the electrochemical performance of nanostructured ZnO films, here, we fabricated flower-like ZnO–CoO–C nanowall arrays for lithium-ion batteries. The arrays showed enhanced capacity compared to those of the ZnO and ZnO–C counterparts and the mechanism for the improved performance was discussed.

2. Experimental

The fabrication of flower-like ZnO–CoO–C nanowall arrays was carried out as follows (Scheme 1). At first, zinc films were coated on copper plates by cathodic deposition in an aqueous solution containing ZnO (12 g L^{-1}), NaOH (120 g L^{-1}), and additive 441 (4 mL L^{-1}). The electroplating was performed at current density of 10 mA cm^{-2} at room temperature for 140 s. After electrodeposition, the copper plates were washed with deionized water and dried in air. Then the Zn-coated copper plates were immersed in 80 mL of 0.13 M ammonia ($NH_3 \cdot H_2O$, 25%) at 80 °C for 4 h [13,20,21]. After being rinsing with water, the obtained ZnO nanowall arrays were immersed into 0.1 M $Co(Ac)_2$ aqueous solution for 0.5 h. After being washed with distilled water and dried at 80 °C, the resulting films were heated at 400 °C for 0.5 h under argon atmosphere [20]. The fabrication of ZnO–C nanowall arrays was conducted according to the procedure reported in reference [14].

The assembly and electrochemical measurements of coin cells were carried out according to the procedures described in reference [13]. The mass of active materials loading on an electrode was determined to be 0.5–1.0 mg according to the procedure reported in reference [13].

The morphologies of the nanowall arrays were observed with a Quanta 200 (FEI) scanning electron microscopy (SEM). X-ray diffraction (XRD) analysis was carried out by using an XRD-6000 (Shimadzu). Thermogravimetric analysis (TGA) was performed on powder-form ZnO–CoO–C scraped from the copper substrates through a ZRY-2P thermal analyzer in an air flow at a heating rate of 10 °C min^{-1}.

* Corresponding author. Tel.: +86 451 8641 3721; fax: +86 451 8641 8616.
E-mail address: panqm@hit.edu.cn (Q. Pan).

0925-8388/$ – see front matter © 2011 Elsevier B.V. All rights reserved.
doi:10.1016/j.jallcom.2011.06.114

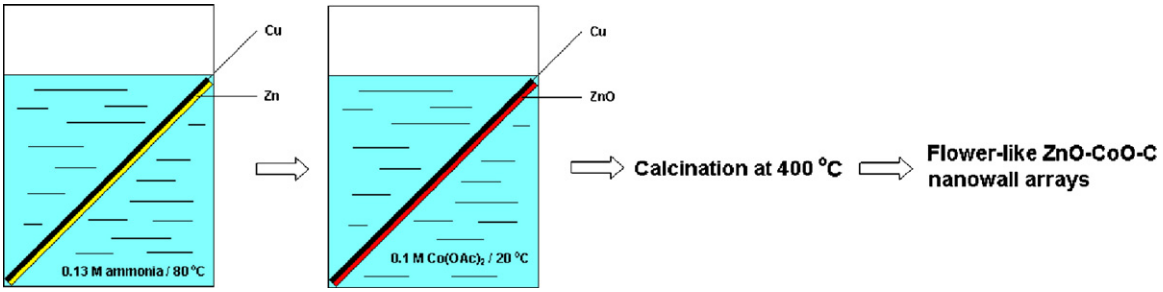

Scheme 1. Illustration for the fabrication of flower-like ZnO–CoO–C nanowall arrays.

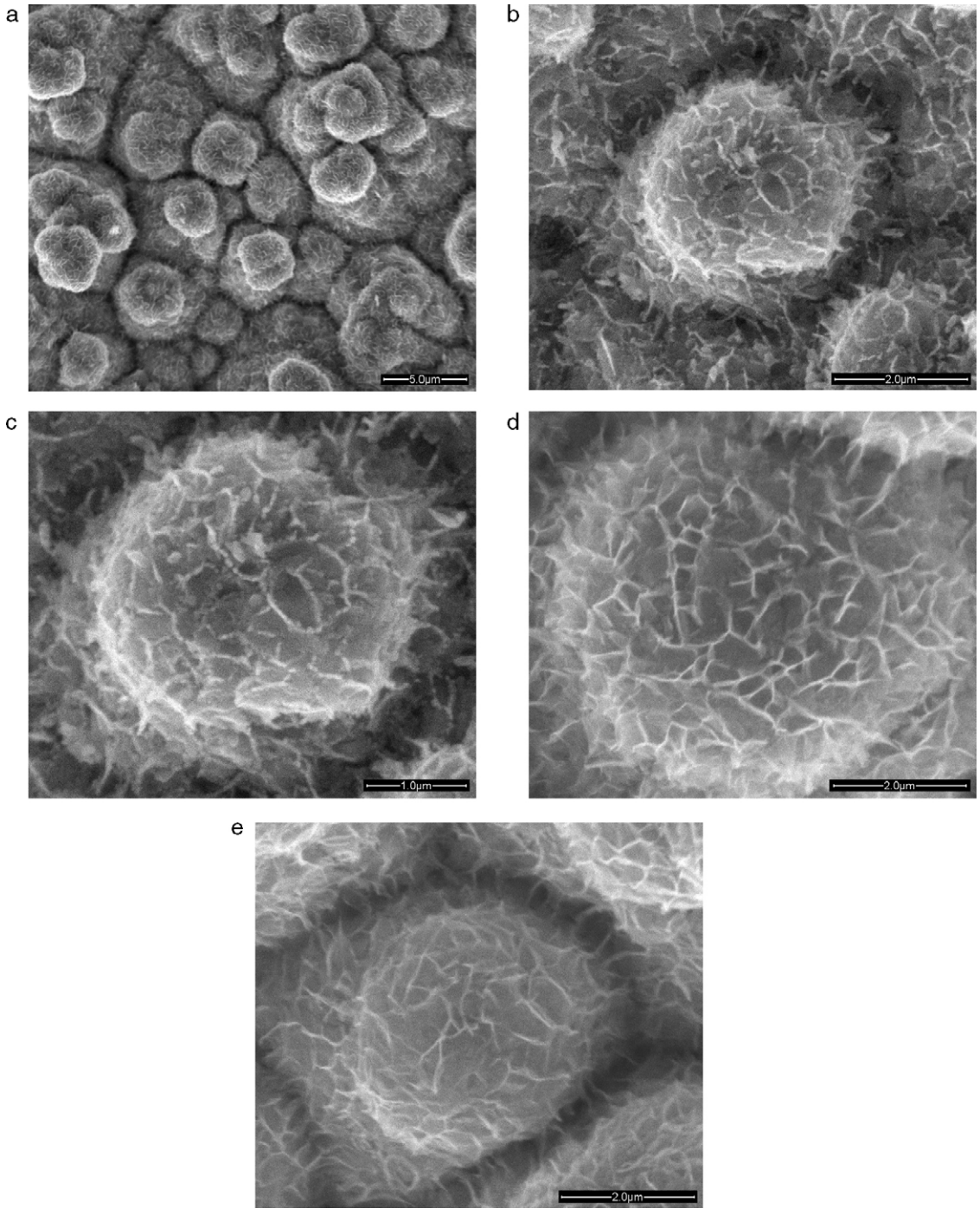

Fig. 1. SEM images of flower-like ZnO–CoO–C (a–c), ZnO (d) and ZnO–C (e) nanowall arrays.

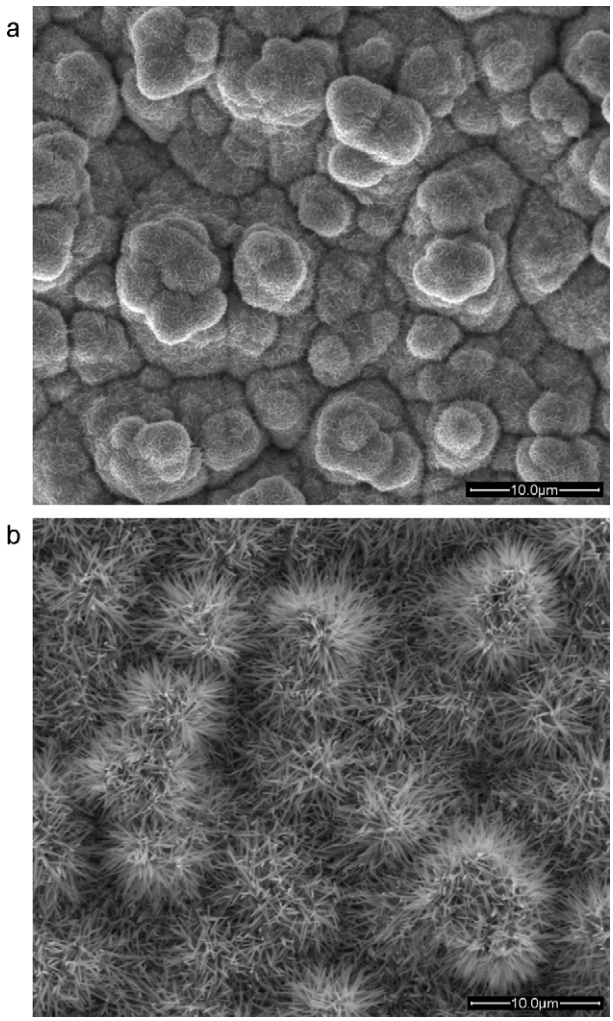

Fig. 2. SEM images of ZnO films prepared in (a) 0.13 M and (b) 0.18 M ammonia solutions.

3. Results and discussion

3.1. Characterization of flower-like ZnO–CoO–C nanowall arrays

Fig. 1 shows the SEM images of the obtained ZnO, ZnO–C and ZnO–CoO–C nanowall arrays. Flower-like microspheres with a diameter about 3–5 μm cover on the surfaces of ZnO-based films, and each flower-like microsphere is built from nanowalls of a few tens nm in thickness. No difference in morphology is observed between ZnO and ZnO–C films (Fig. 1d and e). However, after treatment with cobalt acetate and subsequent calcination, the surfaces of nanowalls become rougher for ZnO–CoO–C arrays (Fig. 1b and c).

We also compared the surface morphology of the present ZnO arrays with those of dandelion-like ZnO arrays prepared in 0.18 M ammonia solution [13]. In contrast, no nanowall instead of nanorods grow on the arrays prepared in 0.18 M ammonia solution (Fig. 2), implying the importance of ammonia concentration on the surface morphologies of the resulting ZnO films.

The chemical composition of the resulting ZnO–CoO–C films was determined by XRD, EDX, XPS and Raman measurements. All XRD patterns of the arrays show feature peaks of ZnO phase (JCPDS 36-1451) [3], except those from copper substrate (Fig. 3a). The particle sizes of ZnO are 19.7, 18.9 and 20.7 nm for ZnO, ZnO–C, and ZnO–CoO–C nanowall arrays, respectively. Although no peak ascribed to CoO or carbon is detected by XRD, EDX and XPS measurements confirm the presence of CoO and carbon phases for ZnO–C and ZnO–CoO–C arrays. EDX plots (Fig. 3b and c) clearly show the existence of cobalt and carbon on ZnO–CoO–C arrays and carbon on ZnO–C arrays. Co 2p spectrum (Fig. 4a) displays the Co 2p3/2 and Co 2p1/2 peaks at 780.1 and 796.6 eV, respectively, which can be assigned to Co atom of CoO phase [22–24]. In addition, Raman spectra of ZnO–CoO–C shows the vibration modes of ZnO at 334, 442, and 583 cm^{-1}; CoO at 463, 503 and 644 cm^{-1}, and carbon at 1383 and 1608 cm^{-1} [20,25].

The carbon content in the arrays was estimated to be 4.7 wt.% for ZnO–CoO–C and 6.9 wt.% for ZnO–C by thermogravimetric analysis (Fig. 5a). TGA was also carried out on CoO–C composite prepared from cobalt acetate under the same calcination conditions as ZnO–CoO–C films. It is observed in Fig. 5b that there is 32.8 wt.% of carbon phase in the CoO–C composite, implying that the weight proportion of CoO and carbon phases in the composite is about 2:1. On the basis of TGA data, one can speculate that the weight proportions of ZnO, CoO and carbon phases in flower-like ZnO–CoO–C arrays approximates 85:10:5. The above results demonstrate the fabrication of flower-like ZnO, ZnO–C and ZnO–CoO–C nanowall arrays on copper foils through solution-immersion and subsequent calcination processes.

3.2. Electrochemical performance of flower-like ZnO–CoO–C nanowall arrays

Fig. 6a shows the voltage profiles of ZnO-based nanowall arrays. Compared to ZnO and ZnO–C arrays, a small voltage plateau appears near 1.15 V in the first lithiation process, which might relate to the reduction of CoO into Co *via* the reaction $CoO + 2Li^+ + 2e^- \rightarrow Co + Li_2O$ [12]. While the plateau at about 0.93 V is ascribed to the reduction of ZnO into Zn and the formation of Li_2O through the reaction $ZnO + 2Li^+ + 2e^- \rightarrow Zn + Li_2O$. ZnO, ZnO–C and ZnO–CoO–C nanowall arrays exhibit the initial lithiation and delithiation capacities of 973.5 and 476.5 mA h g^{-1}, 1161.6 and 625.4 mA h g^{-1}, 1331 and 876.7 mA h g^{-1}, with an initial coulombic efficiency of 48.9, 53.8 and 65.9%, respectively. After discharging and charging for 50 cycles, ZnO–CoO–C arrays still deliver a delithiation capacity of 438 mA h g^{-1}; whereas the capacities of ZnO–C and ZnO arrays are 315.7 and 237.7 mA h g^{-1}, respectively (Fig. 6b).

ZnO–CoO–C films also show desirable high rate capability (Fig. 7), delithiation capacities of 280 and 224 mA h g^{-1} are retained at 1.0 and 2.0 C rates, corresponding to 64.2% and 51.7% of the capacity at 0.5 C, respectively. In contrast, ZnO and ZnO–C arrays only show a reversible capacity of 215.8 and 188.6 mA h g^{-1} at 1.0 C, and 157.2 and 127.6 mA h g^{-1} at 2.0 C, respectively. It is evident that ZnO–CoO–C arrays still deliver higher reversible capacity than ZnO and ZnO–C counterparts at 1.0 and 2.0 C. The high rate capability of ZnO–CoO–C films is believed to arise from the advantages of flower-like nanowall arrays, such as large electrode/electrolyte contact area, short diffusion path for ions and electrons, direct contact between current-collector and electroactive materials, etc. We also compared the present results with those of the reported ZnO-based anodes [3,7–10,13–20]. By comparison, flower-like ZnO–CoO–C nanowall arrays exhibit one of the most desirable capacities and cycling characteristics.

3.3. Mechanism for capacity improvement

To understand the mechanism for the high capacity of ZnO–CoO–C anodes, cyclic voltammetry was conducted on flower-like ZnO, ZnO–C and ZnO–CoO–C nanowall arrays at a scan rate of 0.3 mV s^{-1}, respectively. Compared to ZnO and ZnO–C arrays, two peaks at about 1.1 and 0.88 V are observed for ZnO–CoO–C arrays in the first cathodic scan. The potentials of these peaks are consistent with those of the voltage plateaus on the initial delithia-

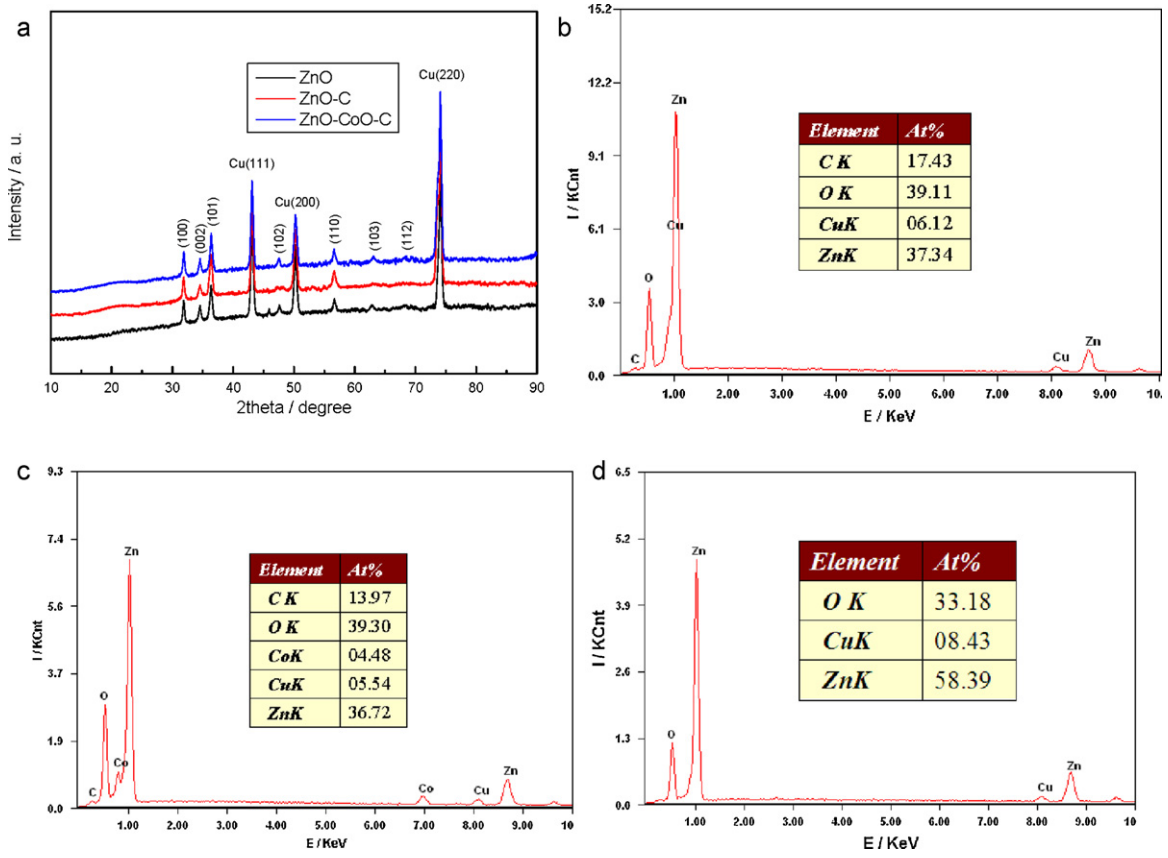

Fig. 3. XRD patterns (a) of ZnO-based nanowall arrays; EDX plots of ZnO–C (b), ZnO–CoO–C (c) and ZnO (d) nanowall arrays.

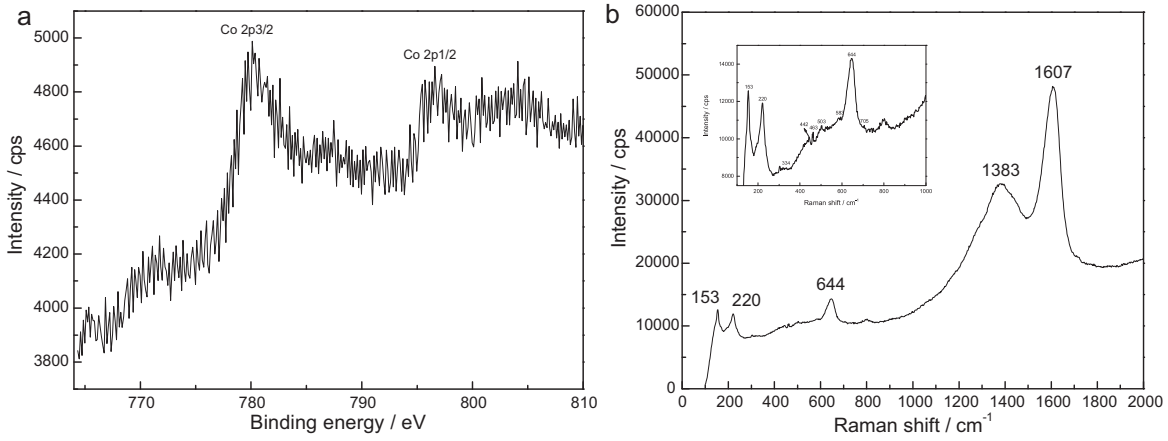

Fig. 4. Co 2p (a) and Raman spectra (b) of ZnO–CoO–C nanowall arrays.

Table 1
Current densities of the anodic peaks at 0.70 and 1.5 V and the capacity distributions associated with these peaks in the first delithiation process.

ZnO-based nanowall arrays	Intensity of anodic peaks at 0.70 and 1.5 V in the first scan (mA)		I_b/I_a	Initial delithiation capacity at 0–1.0 and 1.0–2.0 V (mA h g^{-1})		C_2/C_1
	I_a (0.70 V)	I_b (1.5 V)		C_1 (0–1.0 V)	C_2 (1.0–2.0 V)	
ZnO	0.27	0.26	0.96	193.1	212.8	1.10
ZnO–C	0.18	0.33	1.83	236	264	1.12
ZnO–CoO–C	0.28	0.66	2.35	254.5	442.3	1.74

tion profile of ZnO–CoO–C. As shown in Fig. 8, there is no noticeable difference in the anodic peaks at ~0.70 V that are ascribed to the de-alloying process of Li–Zn alloy among these ZnO-based arrays. However, the intensities of the peaks at ~1.5 V increase in order of ZnO, ZnO–C, and ZnO–CoO–C. Similar results were also observed for Ni coated ZnO [16], $Ni_3ZnC_{0.7}$ incorporated ZnO [19], and flower-like ZnO–NiO–C films [20]. Although the electrical contact between ZnO particles might explain for this intensity increase, electro-

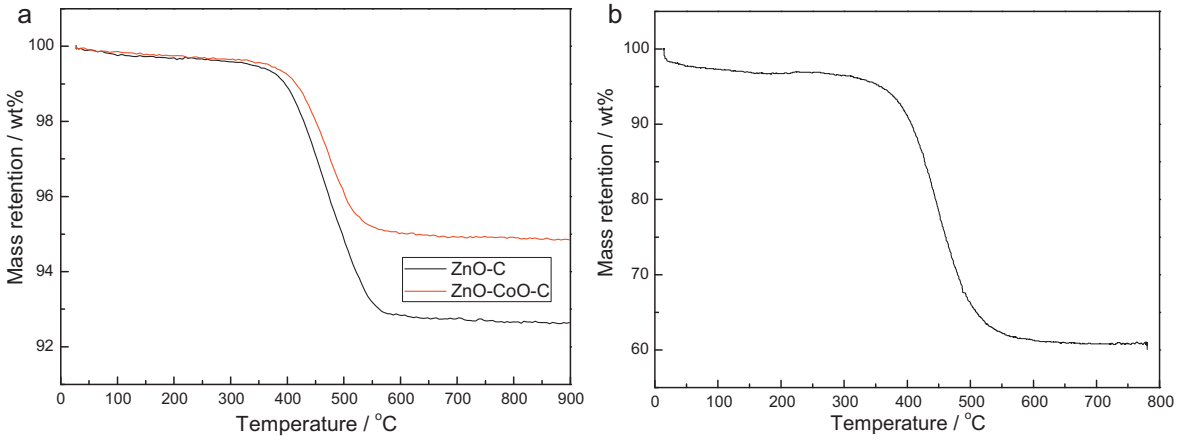

Fig. 5. Thermogravimetric analysis curves of ZnO–C and ZnO–CoO–C nanowall arrays; (b) is the TGA of CoO–C composite prepared under the same calcination conditions like ZnO–CoO–C arrays.

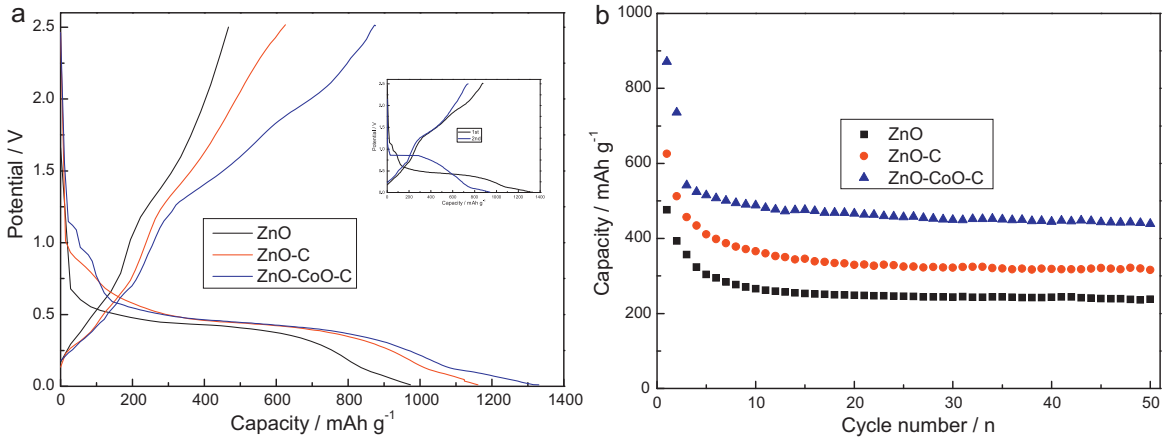

Fig. 6. Voltage profiles (a) and cycling characteristics (b) of the flower-like ZnO, ZnO–C and ZnO–CoO–C nanowall arrays at a rate of 0.5 C. Inset is the initial two lithiation–delithiation curves of ZnO–CoO–C arrays.

chemical impedance spectroscopy shows that there is no great difference in the resistance between ZnO–C and ZnO–CoO–C arrays (Fig. 8d). Because the anodic peaks at 0.70 and 1.5 V relate to different electrochemical processes, we expect that a quantitatively analysis on these peaks might help to understand the mechanism for the capacity improvement of flower-like ZnO–CoO–C nanowall arrays. Here, the current intensity of the anodic peaks at 0.70 and 1.5 V, and the capacity distributions associated with these peaks in the first delithiation process were summarized in Table 1. As seem in Table 1, the intensity of peak at 0.70 V (I_a) exhibits little change, while that of the peak at 1.5 V (I_b) increases from 0.26 to 0.33 and 0.66 for ZnO, ZnO–C, and ZnO–CoO–C, respectively. As a result, ZnO–CoO–C nanowall arrays display the highest I_b/I_a ratio (2.35) compared to ZnO (0.96) and ZnO–C (1.83) counterparts. More interestingly, the capacity C_1 at 0.70 V displays slightly increase in order of ZnO, ZnO–C and ZnO–CoO-–C arrays; while the capacity C_2 at 1.5 V increases remarkably for ZnO–CoO–C arrays compared to those of ZnO and ZnO–C arrays. Consequently, the capacity ratio of C_2/C_1 enhances in order of ZnO (1.10), ZnO–C (1.12) and ZnO–CoO–C (1.74). Reasonably, the enhanced capacity at 0.70 and 1.5 V for ZnO–C nanowall arrays can be ascribed to the conducting effect of carbon phase. Considering that the capacity ratio C_2/C_1 of ZnO–C arrays is similar to that of ZnO arrays, one can conclude that the carbon phase contributes equally to the capacities at 0.70 and 1.5 V, respectively. Compared to ZnO–C, however, the capacity at 1.5 V enhances from 264 to 442.3 mA h g^{-1} for ZnO–CoO–C arrays,

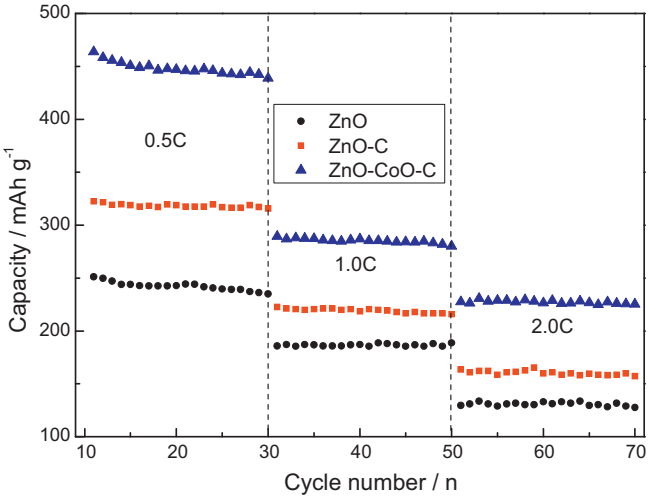

Fig. 7. Rate capability of flower-like ZnO, ZnO–C and ZnO–CoO–C nanowall arrays.

and capacity ratio C_2/C_1 increases from 1.12 to 1.74, suggesting the great influence of CoO phase on the capacity at 1.5 V.

To explore the contribution of CoO–C phases to the capacity of ZnO–CoO–C arrays, control experiments were carried out on CoO–C composite prepared from cobalt acetate under the same

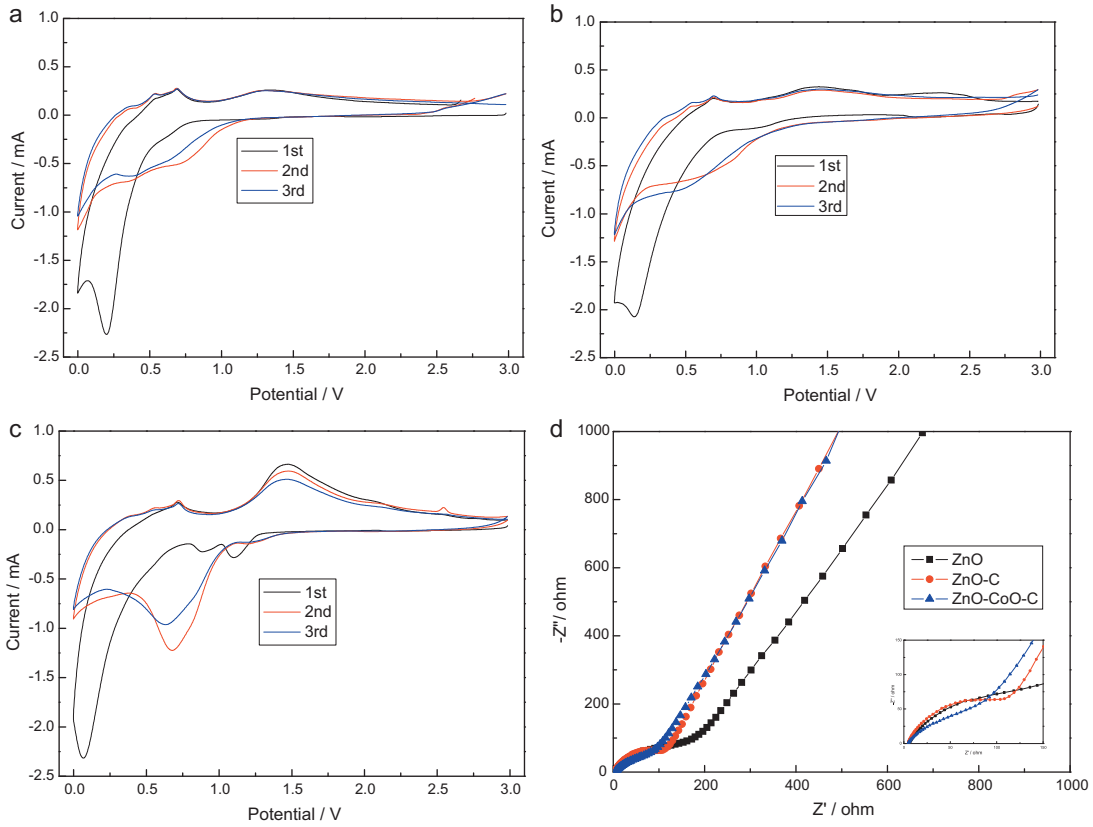

Fig. 8. Cyclic voltammograms of flower-like ZnO (a), ZnO–C (b) and ZnO–CoO-–C (c) nanowall arrays at a scan rate of 0.3 mV s^{-1}, (d) electrochemical impedance spectra recorded on ZnO, ZnO–C and ZnO–CoO–C nanowall arrays at the end of the 50th cycle.

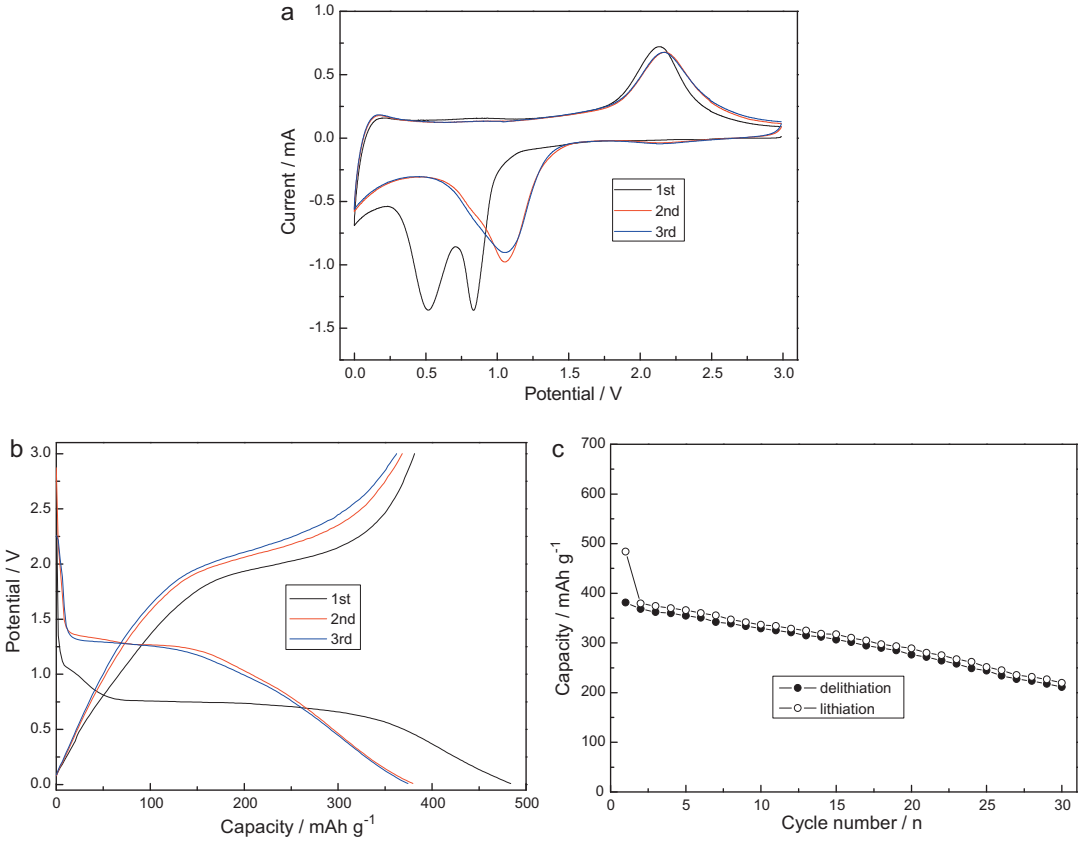

Fig. 9. CV (a), voltage profile (b) and cycling characteristics (c) of CoO–C composite prepared under the similar calcination conditions like ZnO–CoO–C arrays.

calcination conditions as those of ZnO–CoO–C films, and the resulting composite was investigated by thermogravimetric analysis and electrochemical measurements (Fig. 9). TGA curve shows that the content of carbon and CoO in the composite is about 32.8 and 67.2 wt.% (Fig. 5b). And CV results display that the main electroactive materials in the composite is carbon and CoO (Fig. 9a). However, the initial delithiation capacity of CoO–C composite is only 381 mA h g^{-1} and the capacity decreases to 211 mA h g^{-1} at the 30th cycle (Fig. 9b and c). Considering that the content of CoO and carbon phases in ZnO–CoO–C is less than 20 wt.%, these results imply that a simple combination of ZnO and CoO–C composite can not reach the high capacity of ZnO–CoO–C arrays (e.g. 438 mA h g^{-1} at the 50th) under our experimental conditions. In other words, CoO and C phases contribute little capacity to the flower-like ZnO–CoO–C arrays.

Above results indicate that other reason is responsible for the high capacity at 1.5 V. Generally, the electrochemical process at ~1.5 V is mainly ascribed to the decomposition of Li_2O *via* reaction $Zn + Li_2O \rightarrow 2Li^+ + ZnO + 2e^-$ [14,16,20], and the factor that facilitates Li_2O decomposition will improve the reversible capacity of ZnO anodes. Recent studies showed that deposition of metal nanoparticles such as Ni and Au could improve the capacity of ZnO and Co_3O_4 anodes due to the catalytic effects of the metal phases on Li_2O decomposition [16,26]. In the present case, it is believed that Co phase forms *via* the reaction $CoO + 2Li^+ + 2e^- \rightarrow Co + Li_2O$ in the initial lithiation process [12,27–29], which might acts as a catalyst for Li_2O decomposition and partly increase the reversible capacity of ZnO–CoO–C nanowall arrays (as evidenced by the enhanced intensity of the anodic peak at 1.5 V). Therefore, although the capacity associated with CoO–C phases is limited, we can not ignore the Co phase produced in the first lithiation process and its contribution to the capacity of ZnO–CoO–C arrays.

4. Conclusions

In summary, flower-like ZnO–CoO–C nanowall arrays as anodes of lithium-ion batteries were fabricated through simple solution-immersion steps and subsequent heat treatment at moderate temperature, and they exhibited high reversible capacity of 437 mA h g^{-1} and rate capability of 224 mA h g^{-1} at 2.0 C. It was revealed that the surface morphology and chemical composition of the ZnO-based arrays had an important impact on their lithium storage capacity. The mechanism for the high capacity of ZnO–CoO–C nanowall arrays was believed to arise from the catalytic effect of Co phase on the decomposition of Li_2O and the conducting carbon layer formed on ZnO nanowalls. The results of this study suggest a strategy for improving the electrochemical properties of transition metal oxides in lithium-ion batteries based on the morphology and composition manipulation.

Acknowledgement

This study was financially supported by National Natural Science Foundation of China (Grant No. 50803013).

References

[1] J.B. Goodenough, Y. Kim, Chem. Mater. 22 (2010) 587.
[2] J.M. Tarascon, Chem. Mater. 22 (2010) 724.
[3] Z.W. Fu, F. Huang, Y. Zhang, Y. Chu, Q.Z. Qin, J. Electrochem. Soc. 150 (2003) A714.
[4] J. Wang, P. King, R.A. Huggins, Solid State Ionics 20 (1986) 185.
[5] H. Li, X. Huang, L. Chen, Solid State Ionics 123 (1999) 189.
[6] M. Baibarac, I. Baltog, T. Velula, I. Pasuk, S. Lefrant, N. Gautier, J. Phys.: Condens. Matter. 21 (2009) 445801.
[7] F. Belliard, J.T.S. Irvine, J. Power Sources 97–98 (2001) 219.
[8] Z.F. Zheng, X.P. Gao, G.L. Pan, J.L. Bao, J.Q. Qu, F. Wu, D.Y. Song, Chin. J. Inorg. Chem. 20 (2004) 488.
[9] J.P. Liu, Y.Y. Li, X.T. Huang, IEEE Xplore: INEC 1–3 (2008) 53.
[10] Y.H. Tong, J. Cheng, J.Q. Deng, G.G. Siu, J. Electrochem. Soc. 156 (2009) K82.
[11] l. Hochbaum, P.D. Yang, Chem. Rev. 110 (2010) 527.
[12] Y.G. Li, B. Tan, Y.Y. Wu, Nano. Lett. 8 (2008) 265.
[13] H.B. Wang, Q.M. Pan, Y.X. Chen, J.W. Zhao, G.P. Yin, Electrochim. Acta 54 (2009) 2851.
[14] J.P. Liu, Y.Y. Li, R.M. Ding, J. Jiang, Y.Y. Hu, X.X. Ji, Q.B. Chi, Z.H. Zhu, X.T. Huang, J. Phys. Chem. C 113 (2009) 5336.
[15] W.D. Zhang, B. Xu, L.C. Jiang, J. Mater. Chem. 20 (2010) 6383.
[16] C.Q. Zhang, J.P. Tu, Y.F. Yuan, X.H. Huang, X.T. Chen, F. Mao, J. Electrochem. Soc. 154 (2007) A65.
[17] G.F. Yan, H.S. Fang, G.S. Li, Chin. J. Struct. Chem. 28 (2009) 409.
[18] X.D. Tang, Q.M. Pan, J. Liu, J. Electrochem. Soc. 157 (2010) A55.
[19] J.H. Lee, M.H. Hon, Y.W. Chung, I.C. Leu, Appl. Phys. A - Mater. Sci. Process. 102 (2011) 545.
[20] Q.M. Pan, L.M. Qin, J. Liu, H.B. Wang, Electrochim. Acta 55 (2010) 5780.
[21] Q.M. Pan, Y.X. Cheng, Appl. Surf. Sci. 255 (2009) 3904.
[22] L. Soriano, M. Abbate, A. Fernandez, A.R. Gonzalez-Elipe, F. Sirotti, J.M. Sanz, J. Phys. Chem. B 103 (1999) 6676.
[23] M. Oku, Y. Sato, Appl. Surf. Sci. 55 (1992) 37.
[24] M. Hassel, H.J. Freund, Surf. Sci. Spectra 4 (1996) 273.
[25] J.B. Yi, J. Ding, J. Magn. Magn. Mater. 303 (2006) 160.
[26] K.T. Nam, D.W. Kim, P.J. Yoo, C.Y. Chiang, N. Meethong, P.T. Hammon, Y.M. Chiang, A.M. Belcher, Science 312 (2006) 885.
[27] G.X. Wang, Y. Chen, K. Konstantinov, M. Lindsay, H.K. Liu, S.X. Dou, J. Power Sources 109 (2002) 142.
[28] D. Larcher, G. Sudant, J.B. Leriche, Y. Chabre, J.M. Tarascon, J. Electrochem. Soc. 149 (2002) A234.
[29] G.X. Wang, Y. Chen, K. Konstantinov, J. Yao, J.H. Ahn, H.K. Liu, S.X. Dou, J. Alloys Compd. 340 (2002) L5.